RAA 2021 Vol. **21** No. **5**, 115(9pp) doi: 10.1088/1674-4527/21/5/115

http://www.raa-journal.org *http://iopscience.iop.org/raa*

***R**esearch in*
***A**stronomy and*
***A**strophysics*

Absolute parameters and observed flares in the M-type detached eclipsing binary 2MASS J04100497+2931023

Gang Meng (孟刚)[1], Li-Yun Zhang (张立云)[1,2⋆], Qing-Feng Pi (皮青峰)[3], Liu Long (龙柳)[4], Xianming L. Han (韩先明)[5,1] and Misra Prabhakar[6]

[1] College of Physics & Guizhou Provincial Key Laboratory of Public Big Data, Guizhou University, Guiyang 550025, China; *liy_zhang@hotmail.com*
[2] Key Laboratory for the Structure and Evolution of Celestial Objects, Chinese Academy of Sciences, Kunming 650011, China
[3] College of Medicine, Guizhou University of Traditional Chinese Medicine, Guiyang 550025, China
[4] Department of Astronomy, Beijing Normal University, Beijing 100875, China
[5] Dept. of Physics and Astronomy, Butler University, Indianapolis, IN 46208, USA
[6] Department of Physics & Astronomy, Howard University, Washington DC 20059, USA

Received 2020 October 30; accepted 2020 December 1

Abstract The eclipsing binary 2MASS J04100497+2931023 (J04100497+2931023) is classified its spectral type of M0±2V on basis of a low-resolution spectral survey by the Large Sky Area Multi-Object Fiber Spectroscopic Telescope (LAMOST). The low-resolution spectra exhibit strong single-peak emission in the Hα line. We obtained the radial velocities of this binary by means of the Cross-Correlation Function method from the LAMOST medium-resolution spectra. Both components of J04100497+2931023 indicate strong emissions in the Hα line. We performed follow-up photometric observations of J04100497+2931023 using the Xinglong 85 cm telescope of National Astronomical Observatories, Chinese Academy of Sciences. We obtained its full light curve in VRI filters. We first determined their absolute parameters from simultaneously radial velocity and light curves by the Wilson-Devinney program. From our new light curves, we detected three flares for the first time, including one convective flare. The amplitudes, durations, energies, and spectral indices of three flares were also determined. J04100497+2931023 was monitored for approximately 29 h, which indicates that the flare rate is 0.1 flare per hour. We conclude that J04100497+2931023 is a low-mass detached eclipsing binary with strong magnetic activity.

Key words: binaries: eclipsing — stars: flare — star: low-mass — stars: J04100497+2931023

1 INTRODUCTION

Low-mass stars are the majority in the Milky Way. However their properties and regularities are still unclear because of their low luminosity. It is important to determine the orbital parameters of low mass eclipsing binaries to understand the discrepancies between stellar observations and evolutionary models (Baraffe et al. 1998; Ribas et al. 2008). Photometric and spectroscopic observations are very useful for studying the flare event, chromospheric activity (Vida et al. 2009; Šmelcer et al. 2017) and period variation (Wolf et al. 2018). The Large Sky Area Multi-Object Fiber Spectroscopic Telescope (LAMOST) is a 4-m Schmidt optical telescope designed for low- and medium-resolution spectral surveys (Cui et al. 2012) at the National Astronomical Observatories, Chinese Academy of Sciences (NAOC). We can also study their chromospheric activity by using the Balmer lines, and Ca II H&K lines (Zhang et al. 2018), and stellar parameters by LAMOST spectroscopic observations (Qian et al. 2018). LAMOST started a new five-year medium-resolution spectroscopic survey since September 2018 and provided the Hα line profile and radial velocity with error less than 1 km s^{-1} (Liu et al. 2020). It is important to study stellar atmospheric parameters and chromospheric activity of eclipsing binaries (Zhang et al. 2020; Qian et al. 2020). From a spectral survey, we found that many newly identified low-mass eclipsing binaries are active. We plan to observe these objects using domestic telescopes with

⋆ Corresponding author

1-m aperture. We can obtain their CCD light curves and discuss their starspot parameters and flare events by using the light curve variability.

Stellar flares are a unique source of information on stellar magnetic activity. Flare events received increasing attention as space telescopes were developed. Hawley et al. (2014) analyzed the flare events and Hα emission of several low-mass M dwarfs using Kepler short cadence data and spectra obtained by using Astrophysical Research Consortium 3.5 m telescope. They found that there are strong correlations among the flare amplitude, duration and energy of GJ 1243. Davenport et al. (2014) examined the largest samples of flares, which consisted of about 6100 individual events for GJ 1243 from 1 minute cadence data from Kepler survey. They found that 80% of multi-peaked and complex flares have durations of 50 min or longer. Lurie et al. (2015) analyzed the flare occurrence rates and starspot evolution of two active M5 stars GJ1245 AB. They also obtained the flare rates and starspot evolution on long time scales. Silverberg et al. (2016) carried out simultaneous Kepler photometric and ground-based spectroscopic observation to extend the constraints on radiative hydrodynamic flare models to a lower-energy regime. Lu et al. (2019) found that the flare frequency of M stars is consistent with the ratio of the activities of certain chromospheric activity indicators as a function of spectral type for M0-M3.

Photometric time-domina data from an extrasolar planets survey revealed that J04100497+2931023 is an eclipsing binary, which determined its period of about approximately 0.607846 days (Devor et al. 2008). To date, no astronomers have studied the magnetic activity of J04100497+2931023. We present new photometric data and LAMOST spectra. The Wilson-Devinney (W-D) program is used to revise the orbital parameters (Wilson 1979, 1990, 1994, 2008). We also discuss the flare events, and determine the chromospheric activity by using the LAMOST spectra.

2 LAMOST LOW AND MEDIUM RESOLUTION SPECTRAL OBSERVATIONS

LAMOST released a low-resolution (approximately 1800) and medium-resolution (about 7500) spectral surveys (Luo et al. 2015; Liu et al. 2019; Wang et al. 2019). We cross-matched J04100497+2931023 with LAMOST DR7[1], and obtained four LAMOST spectra on 2011 October 10, and 2014 January 5 and 25. The observational parameters of J04100497+2931023 are listed in Table 1 (Luo et al. 2015). The fundamental parameters were obtained by fitting model spectra to the observations (Wu et al. 2011). The equivalent widths (EWs) and heights of the Hα line were calculated using IRAF software[2]. There is emission in the Hα line in Figure 1. Because these are low-resolution spectra, it is difficult to distinguish the spectra of the primary and secondary components. We also plot the EWs, along with the orbital phase and heliocentric Julian date (HJD) in Figure 1. The chromospheric activity exhibits short-term (several months) and long-term (three years) scale variations.

The LAMOST medium-resolution spectral survey began in September 2017. The wavelength ranges are 4950 $\sim$ 5350 Å in the blue region and 6300 $\sim$ 6800 Å in the red region (Liu et al. 2020). As the blue region of the LAMOST survey contains more elements lines, we can obtain more-precision radial velocities. Because the LAMOST red region includes the Hα line, we can study the chromospheric activity (Zhang et al. 2020). We obtained six new medium-resolution spectra of J04100497+2931023 on 2019 January 13, from the DR7 data of LAMOST (Fig. 2). The observational log was listed in Table 2, which includes observational data, temperature, exposure time, HJD, phase, and signal to noise (SN) ratio. We applied the cross-correlation function (CCF) to measure the radial velocities from the spectra. We shifted the solar template spectrum for different radial velocities from –500 to 500 km s^{-1} in steps of approximately 1 km s^{-1} and calculated the CCF values. The peak of the CCF indicates the most likely radial velocity. Finally, we obtained the radial velocities of the primary and secondary components of J04100497+2931023, which are listed in 7th and 8th columns, respectively. Because the spectra are the medium-resolution spectra, two clear emission peaks are easily visible above the continuum in the observed Hα lines. We can identify the two emissions from the primary or secondary components of J04100497+2931023. The Hα EWs and the uncertainties of both components were calculated by integrating them over the emission line using the IRAF task. Because the emission of both components shows litter blending, the Hα EWs and heights of the primary and secondary components were measured using two Gaussian fits. This method was also utilized in our previous paper (Zhang & Gu 2008). The results are summarized in Table 2, where the total Hα EWs of both components, primary and secondary components are listed in the 9th, 10th and 11th columns, respectively. The Hα lines of both components of J04100497+2931023 clearly indicate chromospheric activity. Figure 3 shows Hα EWs and heights of total and those of each components. The Hα EWs of J04100497+2931023 are consistent

[1] http://dr7.lamost.org/

[2] IRAF (http://iraf.noao.edu/) is distributed by the National Optical Astronomy Observatories, which are operated by the Association of Universities for Research in Astronomy, Inc., under cooperative agreement with the National Science Foundation.

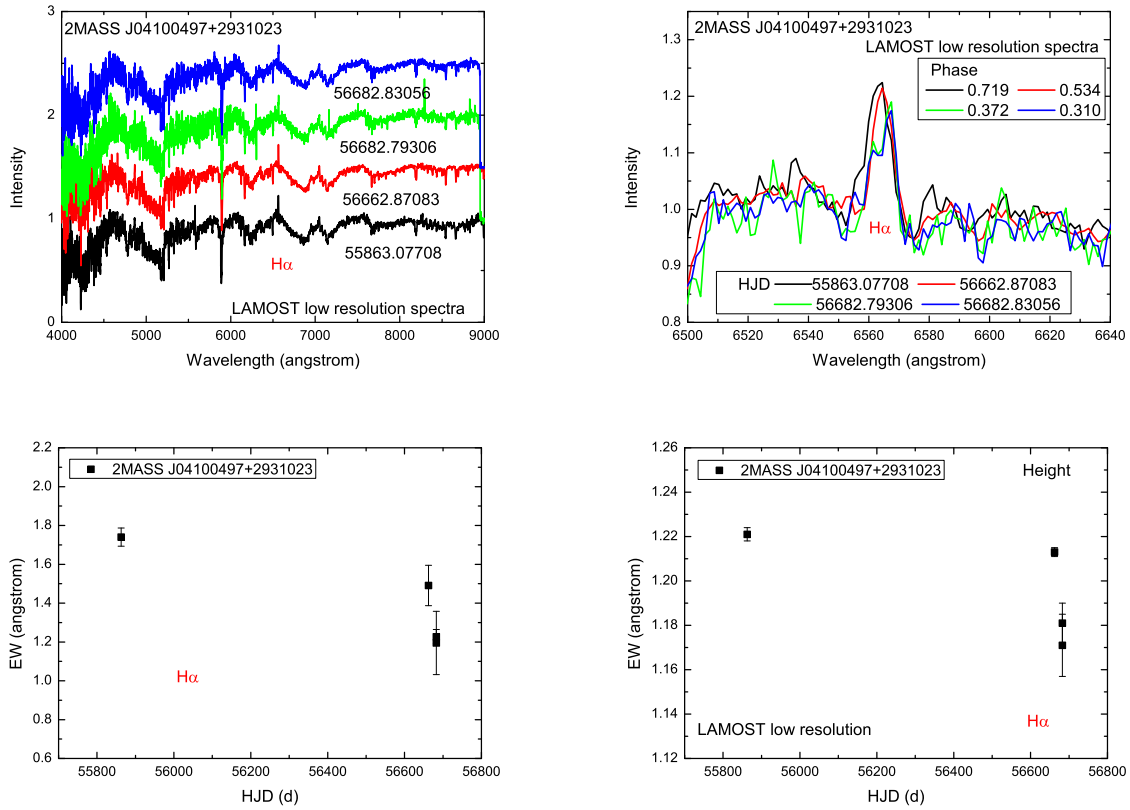

Fig. 1 LAMOST low resolution spectra of J04100497+2931023 and their EWs of intensity and height in Hα line.

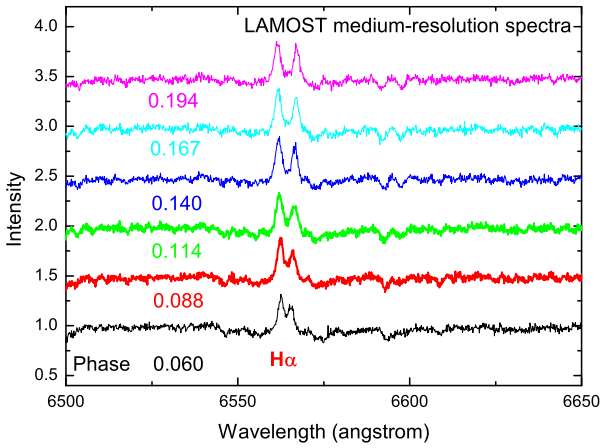

Fig. 2 LAMOST medium-resolution spectra of J04100497+2931023.

Table 1 Spectroscopic Log of LAMOST Low Resolution Survey of J04100497+2931023, and its Hα EWs and Heights

Date	HJD(24,00000+) d	Exposure s	Phase	SN	Sp	Intensity Hα Å	Height Hα Å
2011/10/28	55863.07708	2700	0.719	95	M0	1.740± 0.047	1.221± 0.003
2014/01/05	56662.87083	1800	0.534	141	M0	1.491± 0.104	1.213± 0.002
2014/01/25	56682.79306	2400	0.310	46	M0	1.227± 0.037	1.181± 0.009
2014/01/25	56682.83056	1800	0.372	64	M0	1.195± 0.163	1.171± 0.014

Table 2 Spectroscopic Log of J04100497+2931023 from LAMOST Medium Resolution Survey and its EWs and Heights

HJD 24,00000+ (1)	Exposure s (2)	Phase (3)	SN (4)	Tem K (5)	logg (6)	RV1 km s^{-1} (7)	RV2 km s^{-1} (8)	EW Hα(Total) Å (9)	EW Hα(S) Å (10)	EW Hα(P) Å (11)	Height Hα(S) Å (12)	Height Hα(P) Å (13)
58497.01917	1200	0.0601	36.8	3923±168	4.64±0.20	–78.3±1.9	66.5±4.2	0.916±0.029	0.544±0.015	0.401±0.008	1.293±0.027	1.182±0.002
58497.03583	1200	0.0875	36.8	4214±144	4.03±0.17	–96.7±1.6	72.4±3.4	1.175±0.033	0.729±0.019	0.479±0.004	1.338±0.007	1.228±0.018
58497.05181	1200	0.1138	36.3	4259±156	4.05±0.19	–109.3±1.8	87.7±2.5	1.239±0.025	0.747±0.019	0.517±0.008	1.327±0.027	1.210±0.003
58497.06778	1200	0.1401	36.3	4287±164	4.14±0.20	–125.8±1.9	98.2±3.6	1.361±0.016	0.827±0.022	0.550±0.011	1.361±0.005	1.283±0.022
58497.08444	1200	0.1675	34.9	4283±169	3.71±0.20	–135.4±1.4	108.5±3.5	1.454±0.014	0.858±0.018	0.610±0.011	1.376±0.004	1.301±0.002
58497.10041	1200	0.1938	36.2	4286±166	3.89±0.20	–144.3±1.8	123.8±4.1	1.407±0.086	0.900±0.009	0.593±0.012	1.329±0.032	1.319±0.020

Total means the EWs of the primary and secondary components of binary. P means the primary component and S means the secondary component.

Table 3 Observational Log of J04100497+2931023, Comparison and Check Stars

Targets	Name	Coordinates(Ra;Dec 2000)	Mag_J	Mag_H	Mag_K	Source
Variable star	J04100497+2931023	04:10:05.02;+29:31:02.0	11.131	10.375	10.133	[1]
Comparison star	2MASS J04100473+2932595	04:10:04.73;+29:32:59.5	11.357	10.931	10.793	[1]
Check star	2MASS J04102532+2933298	04:10:25.30;+29:33:31.0	11.296	10.760	10.627	[1]

[1] Cutri et al. (2003).

Table 4 New VRI Light Curve Data for J04100497+2931023

V Band		R Band		I Band	
HJD(+2400000)	Δ mag	HJD(+2400000)	Δ mag	HJD(+2400000)	Δ mag
58844.93230	1.379	58844.93331	0.908	58844.93408	0.356
58844.93503	1.425	58844.93604	0.934	58844.93681	0.384
58844.93776	1.422	58844.93877	0.969	58844.93955	0.419
58844.94049	1.487	58844.94149	1.010	58844.94228	0.463
...	...	...	...	...	...
58850.21260	1.345	58850.25072	0.840	58850.25765	0.286
58850.21566	1.335	58850.25380	0.845	58850.26072	0.287
58850.21874	1.338	58850.25688	0.853	58850.26380	0.291
58850.22182	1.345	58850.25996	0.843	58850.26688	0.276

The full table is available at `http://www.raa-journal.org/docs/Supp/ms4783Table4.dat`.

with its heights. The primary component exhibits higher chromospheric activity than the secondary component.

3 PHOTOMETRIC FOLLOW-UP OBSERVATIONS

We conducted follow-up CCD observations of J04100497+2931023 in VRI filters on 2019 December 27, 28, and 31, and 2020 January 1 using the 85 cm telescope at the NAOC. The camera is a 1024×1024 pixel CCD camera with a $BVRI$ filter system (Zhou et al. 2009; Bai et al. 2018). The data were processed by using `IRAF`, the procedures included standard stellar aperture photometry. Table 3 shows the parameters of J04100497+2931023, the comparison and check stars. Table 4 lists all the photometric data. The photometric derivations for VRI bands from the observations of the comparison star and check star are 0.005 mag, 0.008 mag, 0.006 mag, respectively. The light curves are shown in Figure 4. In addition, we obtained the VRI light minima times by means of the method described by Kwee & van Woerden (1956), and the averaged values in Table 5, including light minima times, errors, and types. We obtained a new linear ephemeris as follows:

$$\begin{aligned} \mathrm{Min}.I = {} & \mathrm{JD(Hel.)}2458845.26923(\pm 0.00006) \\ & + 0^d.60783(\pm 0.00005)E. \end{aligned} \quad (1)$$

4 ABSOLUTE PARAMETERS DETERMINED BY THE W-D METHOD

First, the orbital parameters were obtained by the updated version of the W-D program (Wilson & Devinney 1971). The solutions were obtained by simultaneously combining with radial velocity and VRI light curves. During the fitting, we set the weights of the data for the flare events to zero. We set the gravity-darkening coefficients to 0.32 (Lucy 1967) and the bolometric albedo to 0.50 for both components (Ruciński 1973). The bolometric and filter limb-darkening coefficients (x_1 and x_2) were set for each filter (van Hamme 1993) in Table 6. Because our radial velocity curves are not complete, we also used the relationship between the residual and mass ratios to estimate the photometric mass ratio. The program operates by changing the parameters to determine the possible values of the photometric mass ratio. After many runs, we obtained the residual results for multiple mass ratios

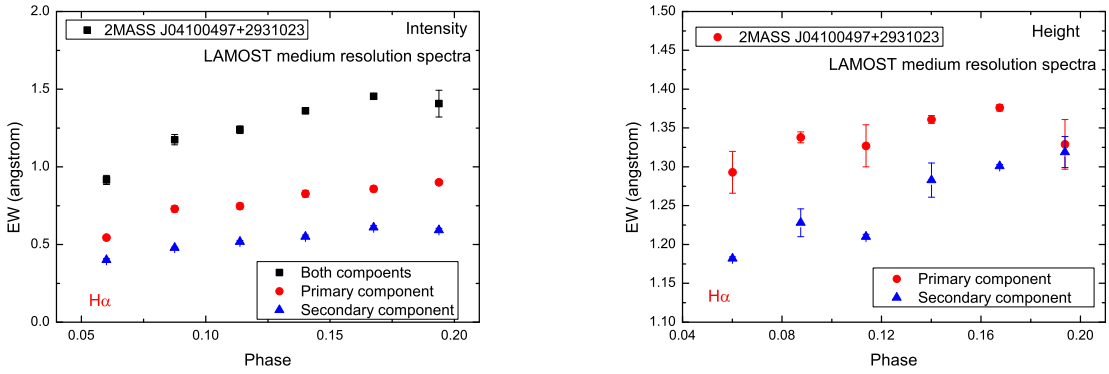

Fig. 3 Hα EWs (*left*) and heights (*right*) of total and those of each component.

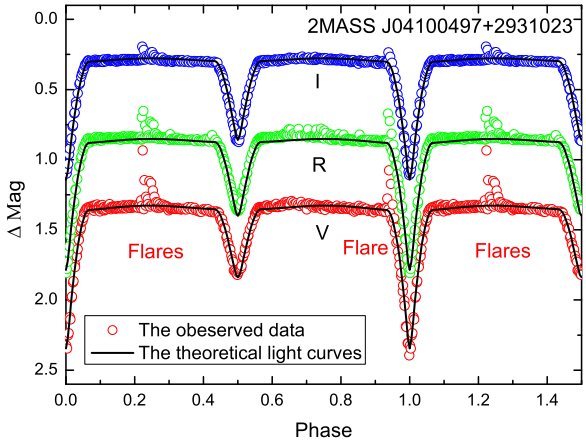

Fig. 4 Theoretical and observed light curves of J04100497+2931023.

Table 5 Newly Obtained VRI Minima Times of J04100497+2931023

HJD (V)	HJD (R)	HJD (I)	HJD (average)	Type
2458844.96489± 0.00191	2458844.96557± 0.00004	2458844.96555± 0.00093	2458844.96534±0.00096	S
2458845.26918± 0.00062	2458845.26916± 0.00052	2458845.26930± 0.00044	2458845.26921±0.00053	P
2458849.21996± 0.00212	2458849.22031± 0.00524	2458849.22012± 0.00229	2458849.22013±0.00322	S
2458850.13206± 0.00227	2458850.13177± 0.00438	2458850.13185± 0.00373	2458850.13189±0.00346	P

(M_2/M_1) to find the lowest fitting residual. The fitting residual is plotted versus the photometric mass ratio (q) in the right panel of Figure 5. The curve shows a clear pattern and the most likely mass ratio for J04100497+2931023 is 1.8. From the low-precision spectra of LAMOST, the spectral type of M0 should belong to the more massive component (the primary), which corresponds to Star 2 of W-D code. Therefore, we fixed T_2=4209 K and adjusted the temperature of the primary component T_1. After many runs, we obtained a spectroscopic mass ratio of 1.79(±0.01). The theoretical and observed radial velocity curves of J04100497+2931023 are plotted in the left panel of Figure 5. Fortunately, the spectroscopic mass ratio obtained by fitting the radial velocity data is similar to the photometric mass ratio using q-search from the photometric data. Because the radial velocity curve is not complete, more spectroscopic observations are needed to improve it. The temperature of the secondary component (T_2), inclination (i), the monochromatic luminosity ratios of the primary (L_1) and secondary component (L_2), and the potentials of both components were obtained. The resulting theoretical light curve is superimposed over the data from the three filters of J04100497+2931023 in Figure 4. The final parameters are listed in Table 6,

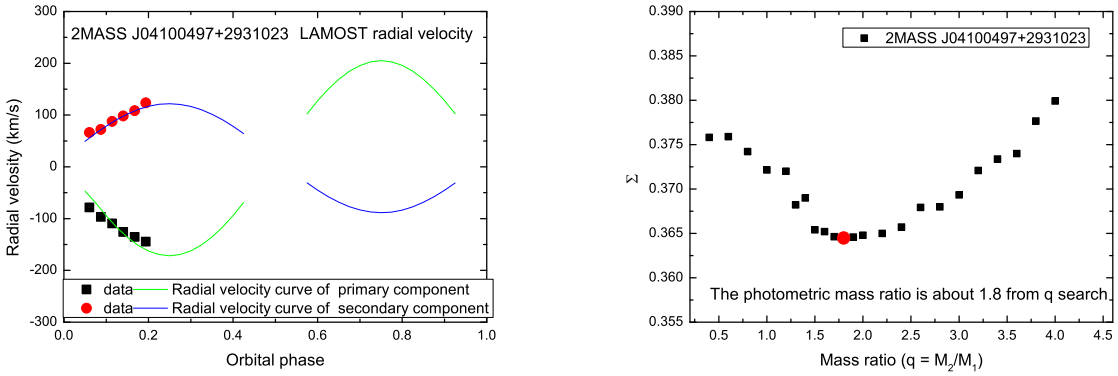

Fig. 5 Theoretical and observed radial velocity curves of J04100497+2931023 (*left*), and relationship of residual and mass ratio (*right*) using the photometric data.

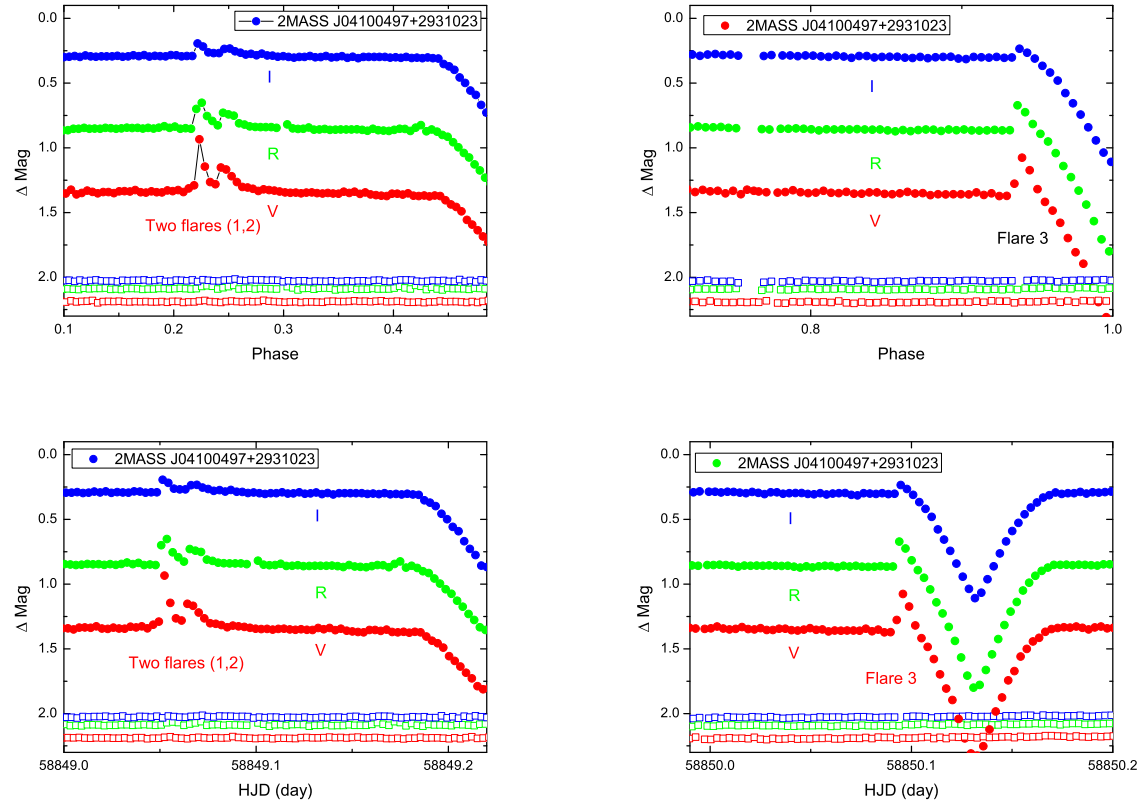

Fig. 6 Three flare events of J04100497+2931023 in phase (*top*) and time (*bottom*), where the flares are identified by numbers. The *solid symbols* represent the different magnitude between J04100497+2931023 and the comparison star, while the *open symbols* represent the difference magnitude between he check star and comparison star. Different colors represent different observational filters. The appearances of the three flares under each filters are consistent with each other.

where the errors of our parameters are small. They are not real errors and computed from the W-D program (Prsa & Zwitter 2005).

5 DISCUSSION AND CONCLUSION

We determined the chromospheric activity of J04100497+2931023 using the LAMOST low- and medium-resolution spectra. Then, we obtained

Table 6 Parameter Values of J04100497+2931023 Obtained Using the Wilson-Devinney Program

Parameters	Generated Values
SYSTEMIC RADIAL VELOCITY(km s^{-1})	17±4
a	3.55±0.15
$M_1(M_\odot)$	0.587±0.006
$M_2(M_\odot)$	1.049±0.011
$R_1(R_\odot)$	0.74±0.04
$R_2(R_\odot)$	0.68±0.04
T_1	4500±6K
Bol1	0.493
Bol2	0.429
X_{1V}	0.779
X_{2V}	0.705
X_{1R}	0.657
X_{2R}	0.612
X_{1I}	0.523
X_{2I}	0.476
T_2	4209±161K
ω_1	6.633 ± 0.032
ω_2	9.960 ± 0.085
$i(^o)$	89.1 ± 0.2
$q\ (M_2/M_1)$	1.79± 0.01
$L_{1V}/(L_{1V}+L_{2V})$	0.659±0.006
$L_{1R}/(L_{1R}+L_{2R})$	0.632±0.006
$L_{1I}/(L_{1I}+L_{2I})$	0.609±0.006
r_1 (Pole)	0.2048 ±0.0014
r_1 (Point)	0.2137 ±0.0017
r_1 (Side)	0.2073 ±0.0015
r_1 (Back)	0.2119 ±0.0016
r_2 (Pole)	0.1906 ±0.0017
r_2 (Point)	0.1930 ±0.0018
r_2 (Side)	0.1917 ±0.0017
r_2 (Back)	0.1927 ±0.0018
σ	0.371

the photometric follow-up light curves for J04100497+2931023 in the VRI bands for the first time. This study also presents the first in-depth study of flare events in the J04100497+2931023 system.

5.1 Orbital Parameters and Chromospheric Activity

We revised the period to 0.60783±0.00005 days for J04100497+2931023, which is in good agreement with previously reported studies (Devor et al. 2008). We firstly obtained the absolute parameters and chromospheric activity of J04100497+2931023. The orbital semi-major axis and systemic radial velocity of J04100497+2931023 are 3.55±0.15 $R\odot$ and 17±4 km s^{-1}, respectively. The inclination of J04100497+2931023 is 89.1 ± 0.2. Both components of J04100497+2931023 show strong chromospheric activity in the Hα line. The chromospheric activity shows short- and long-term variations, especially a short time variation on a time scale of about 20 min. More photometric and spectroscopic observations are very desirable to understand the relationship between photospheric and chromospheric activity.

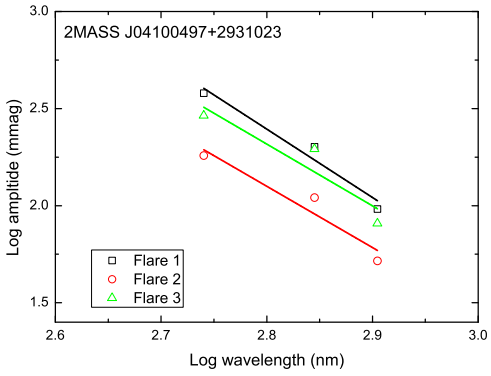

Fig. 7 Spectral index of flares for J04100497+2931023.

5.2 Flare Events

Stellar flares are sudden and interesting events, in which hot gas is ejected into the outer atmosphere of a star and the accumulated magnetic energy is released (Qian et al. 2012). The traditional bolometric energy is in the range of $10^{24} - 10^{27}$ J (Pettersen 1989). We detected three new flares using flare detection criteria similar to in our previous paper (Zhang et al. 2014). The three flares are plotted in Figure 6. The first flare was observed on 2019 December 31, with a maximum value in phase 0.223, a V amplitude of approximately 0.380 mag, and a flare duration of about 21.312 min (Table 7). Notably, there is a convective flare in the left panel of Figure 6, as indicated by two rapid rises and slowly decrease in the light curve of the flare. For two flares in phases 0.223 and 0.245, it is difficult to estimate the flare occurring in the more massive or less massive components. For the third flare in phase 0.939, the primary component (less massive) is eclipsed by the secondary star (more massive). The third flare might occur in the more massive component. Complex flares have also been observed in other M stars (Qian et al. 2012; Davenport et al. 2014). The total duration of the convective flare was approximately 55.4 min. The third flare was observed in the V filter. It had a duration of approximately 22 min and an amplitude of 0.291 mag. Because J04100497+2931023 was monitored for approximately 29 h, the flare rate is about 0.1 flares per hour. We collected all the flare rates of low-mass eclipsing binary in Table 8. Our result is similar to the values of 0.09 for BX Tri (Luo et al. 2019; Dimitrov & Kjurkchieva 2010), 0.06 for GJ 3236 (Šmelcer et al. 2017) and 0.064 for DV Psc (Pi et al. 2019).

To estimate the energy of the flares, we used the Planck law of energy distribution (Šmelcer et al. 2017; Parimucha et al. 2016). The spectral type of J04100497+2931023 was determined to be M0. The

Table 7 Parameters of Newly Observed VRI Flares of J04100497+2931023

Date	No.	HJD	Phase	Flare parameters					Spectra index
d		d		Amplitude	Total time	Rise	Decay	Energy	
d		d		mag	min	min	min	10^{26}J	
20191231	Flare1$_V$	2458849.05236	0.223	0.380	21.312	8.525	12.787	13.13	–3.5±0.7
	Flare1$_R$	2458849.05236	0.223	0.201	21.326	8.539	12.787	9.57	
	Flare1$_I$	2458849.05236	0.223	0.096	21.312	4.262	17.050	5.68	
20191231	Flare2$_V$	2458849.06545	0.245	0.181	34.114	4.277	29.837	10.93	–3.2±0.8
	Flare2$_R$	2458849.06545	0.245	0.110	29.866	4.277	25.589	7.64	
	Flare2$_I$	2458849.06545	0.245	0.052	29.866	8.554	21.312	4.40	
20200101	Flare3$_V$	2458850.09575	0.939	0.291	22.133	8.842	13.291	10.85	–3.2±1.2
	Flare3$_R$	2458850.09575	0.939	0.196	17.712	4.435	13.277	7.77	
	Flare3$_I$	2458850.09575	0.939	0.081	17.698	4.421	13.277	3.38	

Table 8 Flare Ratios of Low Mass M-type Binaries

Name	Spectral type	Period(d)	Flare Number	Flare ratio	Reference
BX Tri	M dwarf	0.19264	13	0.09	Luo et al. (2019); Dimitrov & Kjurkchieva (2010)
CU Cnc	M 3.5V	2.77147	4	0.05	Qian et al. (2012)
CM Dra	M 4.5V	1.26839	13	0.039	Lacy (1977); Kim et al. (1997); Nelson & Caton (2007); Kozhevnikova et al. (2004)
DV Psc	K4+M	0.30854	21	0.064	Pi et al. (2019)
EC13471-1258	M3.5-4	0.15069	2	0.067	O'Donoghue et al. (2003)
GJ 3236	M4	0.77126	54	0.06	Šmelcer et al. (2017)
YY Gem	dM1+dM1	0.81428	39	0.257	Doyle & Mathioudakis (1990); Doyle et al. (1990); O'Donoghue et al. (2003)
J04100497+2931023	M0+	0.60783	3	0.10	Our paper
TYC 5112-252-1	-	0.97694	2	0.014	Šmelcer et al. (2018)

corresponding parameters of the primary component were obtained M_1 = 0.587±0.006 $M\odot$, R_1 = 0.74±0.04$R\odot$, and L_1 = 0.607±0.002$L\odot$ = 7.68±0.02×10^{25} W. Using the mass ratio, radius ratio, and luminosity ratio, we obtained M_2 = 1.049±0.011 $M\odot$, R_2 = 0.68±0.04 $R\odot$, and L_2 =0.393±0.001$L\odot$ = 4.96±0.01×10^{25} W, respectively. The secondary is more massive than the primary component. We estimated the stellar quiescent luminosity by using the method presented by Parimucha et al. (2016): $L = \int_0^\infty 4\pi R^2 S(\lambda)F(\lambda)d\lambda$, where S is the transmission curve in the observed filter and $F(\lambda)$ is the flux outside of the flare in the observed wavelength λ, R is the radius. We also calculated the total flare energy using the same method (Parimucha et al. 2016) as: E(Flare) = $L_{1+2}\int_{t_B}^{t_E}(10^{-0.4\Delta m(t)} - 1)dt$, where L_{1+2} is the total luminosity of J04100497+2931023 and $\Delta m(t)$ is the magnitude of the flare amplitude. We integrated over the duration of the flare to obtain the energies of the three flares for each filter, as shown in Table 7. The flare energies of J04100497+2931023 are in the range (3.38–13.13) ×10^{26} J, which is similar to that of solar flares (Benz 2017).

We plot the flare amplitude versus wavelength in Figure 7. We also determined the spectral indices of our flares by means of linear fitting. The results are listed in the last column of Table 7. The average slope of the flares is –3.3±0.9. The value is similar to the results of –3.2(0.3) for YY Gem (Gary et al. 2012), and 3.9(0.4) for GJ 3236 (Šmelcer et al. 2017). These results indicate that the flare mechanism in low mass eclipsing binaries is the same.

J04100497+2931023 is an M-type detached eclipsing binary with strong magnetic activity. Its chromospheric emission is consistent with its flare events from light curves. This study may prove useful for understanding the properties of active eclipsing binaries from the LAMOST survey. The magnetic activity was also found in other low mass M-type eclipsing binaries, such as BX Tri (Luo et al. 2019), CU Cnc (Qian et al. 2012), and DV Psc (Pi et al. 2019). More photometric and spectroscopic monitors of low mass eclipsing binaries are needed to examine their statistical properties.

Acknowledgements Our research was supported by the Joint Research Fund in Astronomy (Grant Nos. 11963002, U1631236 and U1431114) under a cooperative agreement between NSFC and CAS. We acknowledge the support of the staff of the Xinglong 85 cm telescope and Cultivation Project for LAMOST Scientific Payoff and Research Achievement of CAMS-CAS.

References

Bai, C.-H., Fu, J.-N., Li, T.-R., et al. 2018, RAA (Research in Astronomy and Astrophysics), 18, 107
Baraffe, I., Chabrier, G., Allard, F., et al. 1998, A&A, 337, 403
Benz, A. O. 2017, Living Reviews in Solar Physics, 14, 2
Çakırlı, Ö. 2013, New Astron., 22, 15
Cui, X.-Q., Zhao, Y.-H., Chu, Y.-Q., et al. 2012, RAA (Research in Astronomy and Astrophysics), 12, 1197
Cutri, R. M., Skrutskie, M. F., van Dyk, S., et al. 2003, VizieR Online Data Catalog, II/246

Davenport, J. R. A., Hawley, S. L., Hebb, L., et al. 2014, ApJ, 797, 122
Devor, J., Charbonneau, D., O'Donovan, F. T., et al. 2008, AJ, 135, 850
Dimitrov, D. P. & Kjurkchieva, D. P. 2010, MNRAS, 406, 2559
Doyle, J. G. & Mathioudakis, M. 1990, A&A, 227, 130
Doyle, J. G., Butler, C. J., van den Oord, G. H. J., et al. 1990, A&A, 232, 83
Gary, B. L., Hebb, L. H., Foote, J. L., et al. 2012, in Society for Astronomical Sciences Annual Symposium, 31, 17
Hawley, S. L., Davenport, J. R. A., Kowalski, A. F., et al. 2014, ApJ, 797, 121
Kim, S.-L., Chun, M.-Y., Lee, W.-B., et al. 1997, Information Bulletin on Variable Stars, 4462, 1
Kozhevnikova, A. V., Kozhevnikov, V. P., Zakharova, P. E., et al. 2004, Astronomy Reports, 48, 751
Kwee, K. K. & van Woerden, H. 1956, Bull. Astron. Inst. Netherlands, 12, 327
Lacy, C. H. 1977, ApJ, 218, 444
Liu, N., Fu, J.-N., Zong, W., et al. 2019, RAA (Research in Astronomy and Astrophysics), 19, 075
Liu, C., Fu, J., Shi, J., et al. 2020, arXiv e-prints, arXiv:2005.07210
Lu, H. P., Zhang, L. Y., Shi, J. R., et al. 2019, ApJS, 243, 28
Lurie, J. C., Davenport, J. R. A., Hawley, S. L., et al. 2015, ApJ, 800, 95
Lucy, L. B. 1967, ZAp, 65, 89
Luo, A.-L., Zhao, Y.-H., Zhao, G., et al. 2015, RAA (Research in Astronomy and Astrophysics), 15, 1095
Luo, C., Zhang, X., Wang, K., et al. 2019, ApJ, 871, 203
Morales, J. C., Ribas, I., & Jordi, C. 2008, A&A, 478, 507
Nelson, T. E. & Caton, D. B. 2007, Information Bulletin on Variable Stars, 5789, 1
O'Donoghue, D., Koen, C., Kilkenny, D., et al. 2003, MNRAS, 345, 506
Parimucha, Š., Dubovský, P., Vaňko, M., et al. 2016, Ap&SS, 361, 302
Pi, Q.F., Zhang, L.Y., Bi, S.L., et al. 2019, ApJ, 877, 75
Pettersen, B. R. 1989, Sol. Phys., 121, 299.
Prša, A., & Zwitter, T. 2005, ApJ, 628, 426
Qian, S.-B., Zhang, J., Zhu, L.-Y., et al. 2012, MNRAS, 423, 3646
Qian, S.-B., Zhang, J., He, J.-J., et al. 2018, ApJS, 235, 5
Qian, S.-B., Zhu, L.-Y., Liu, L., et al. 2020, RAA (Research in Astronomy and Astrophysics), 20, 163
Ribas, I., Morales, J. C., Jordi, C., et al. 2008, Mem. Soc. Astron. Italiana, 79, 562
Ruciński, S. M. 1973, Acta Astronomica, 23, 79
Silverberg, S. M., Kowalski, A. F., Davenport, J. R. A., et al. 2016, ApJ, 829, 129
Šmelcer, L., Červinka, L., Mašek, M., et al. 2018, Open European Journal on Variable Stars, 192, 1
Vida, K., Oláh, K., Kővári, Z., et al. 2009, A&A, 504, 1021
Šmelcer, L., Wolf, M., Kučáková, H., et al. 2017, MNRAS, 466, 2542
van Hamme, W. 1993, AJ, 106, 2096.
Wang, R., Luo, A.-L., Chen, J.-J., et al. 2019, ApJS, 244, 27
Wilson, R. E. & Devinney, E. J. 1971, ApJ, 166, 605
Wilson, R. E. 1979, ApJ, 234, 1054
Wilson, R. E. 1990, ApJ, 356, 613
Wilson, R. E. 1994, PASP, 106, 921
Wilson, R. E. 2008, ApJ, 672, 575
Wolf, M., Kučáková, H., Zasche, P., et al. 2018, A&A, 620, A72
Wu, Y., Luo, A.-L., Li, H.-N., et al. 2011, RAA (Research in Astronomy and Astrophysics), 11, 924
Zhang, L.-Y., Pi, Q.-. feng ., & Yang, Y.-G. 2014, MNRAS, 442, 2620
Zhang, L. Y., Lu, H. P., Han, X. M., et al. 2018, NewA, 61, 36
Zhang, L.-Y., Long, L., Shi, J., et al. 2020, MNRAS, 495, 1252
Zhang, L.-Y., & Gu, S.-H. 2008, A&A, 487, 709
Zhou, A.-Y., Jiang, X.-J., Zhang, Y.-P., et al. 2009, RAA (Research in Astronomy and Astrophysics), 9, 349